Three-Dimensional Spatial Movement of the Mitral Valve

Author: BSc. M.L.Tolhuisen
Medical supervisor: Prof.dr.J.G.Grandjean
Technical supervisors: Dr. S. Misra and ir.G.J.Vrooijink
Process supervisor: Dr.M.Groenier

Stage M2-2
Afdeling Thoraxchirurgie
Technische Geneeskunde
Medical Imaging and Intervention

UNIVERSITEIT TWENTE.

The Surgical Robotics Laboratory of the University of Twente is developing a steerable transcatheter that can be used for cardiac interventions, for example mitral valve reconstruction. To create a static surgical field, closed-looped model-based movement control is used. Hence a dynamic model is needed to create a static surgical field. At this moment, no information of the spatial movement of the mitral annulus is available. The aim of this research is to develop a manual segmentation method and to create 3D dynamic models for the mitral annulus. The method is applied to 20 trans-esophagal echocardiograms which were recorded in the same patient in a single recording session. Orthogonal regression is used to place all segmented annuli in the same initial orientation. The mean coordinates of the segmented annuli are tracked showing the displacement of the annulus in the various directions. Comparative data is created by decreasing the mean coordinates by their mean. A dynamic model was created for the movement in z-direction. For the movement in x- and y- direction no dynamic models were created due to noise in the manual segmentation method.

1 INTRODUCTION

In 2010, in Dutch hospitals the amount of valve surgeries has increased to 5906, compared to 2431 surgeries in 1995[1]. 23.7% of these surgeries included mitral valve surgery. Because mitral valve surgery is still invasive, demand for improvement of the surgical techniques still exists[2]. Researchers are developing minimal invasive techniques which focuses on the use of transapical transcatheters[2,3]. Cheung et al. have presented several articles in which they describe their design, application and evaluation of transapical transcatheter mitral valve implantation[2,4,5].

The Surgical Robotics Laboratory of the University of Twente[6] is developing a steerable transcatheter that can be used for applications that include tissue interventions, for example mitral valve reconstruction[7]. Also, the design will prevent damage to the apical myocardium. The catheter will be used during off-pump surgery and will be inserted into the jugular vein. From there it reaches the mitral valve through the vena cava superior, right atrium and atrial septum. This surgical track is shown in Figure .

To facilitate tissue intervention with the catheter during off-pump surgery, it is essential to create a static surgical environment. Therefore, compensation for
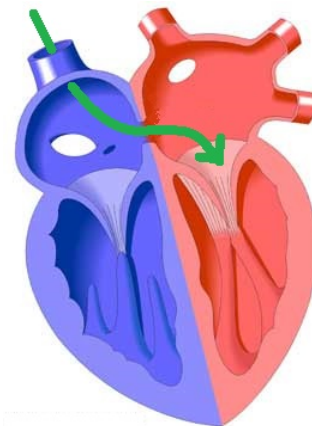

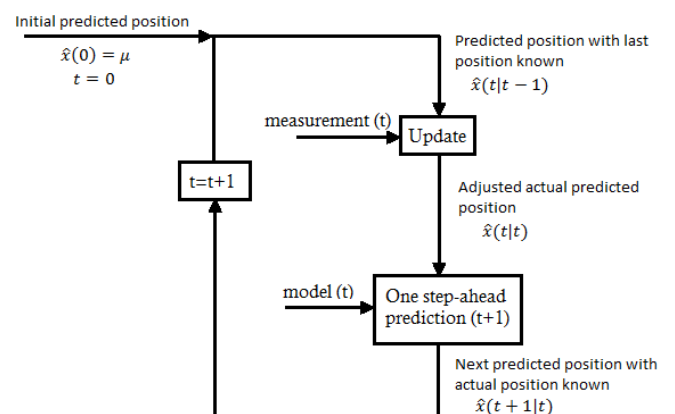*Figure 1 Surgical track of the catheter during mitral valve surgery*

Figure 2 Closed-looped model-based movement control (with t= time, x = three dimensional carthesian position and $\hat{x}$ the prediction of x)

the movement of the surgical field is needed. This is accomplished by the combination of online movement tracking

and modelling. Figure 2 shows a simplified illustration of this closed-looped model based movement control. The model describes the expected movement of the annulus, forming predictions for the subsequent movement. During surgery, online tracking will create updates of the actual movement. For the next prediction the model will be adjusted conform these updates. Therefore, online tracking gives actual movement information, while the dynamic model eliminates delay by predicting the subsequent movement. This enables synchronous movement of the catheter and mitral valve.

Both the online tracking system and dynamic model of the mitral valve has yet to be developed. This research focuses on the creation of the dynamic model. Several researchers describe the dynamic behaviour of the mitral annulus[8–10]. All describe the deformation of the annulus during the cardiac cycle. Yet, no information of the spatial dynamic behaviour is available. The aim of this research is to develop a manual segmentation and analysis method to finally create a dynamical model for the three-dimensional spatial movement of the mitral annulus.
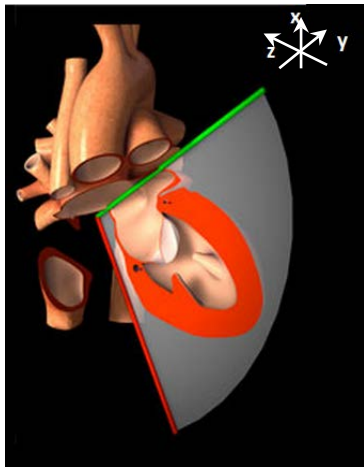

Figure 1 Three dimensional heart model showing cross section of the mitral valve made by a TEE plane (mid-esophageal two chamber view)[17]
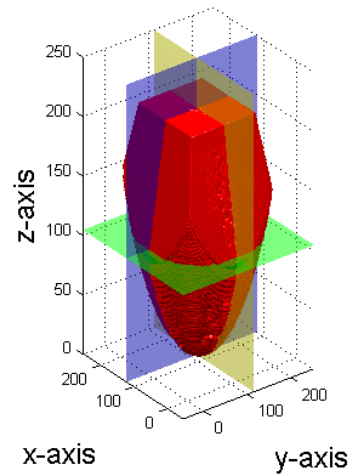

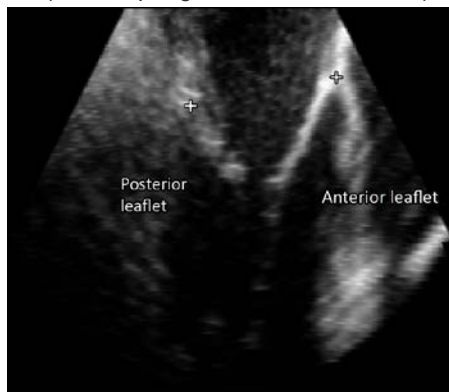*Figure 2 3D TEE cone containing the field of view*

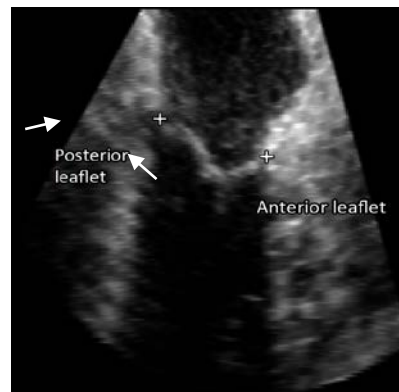*Figure 3 XZ-plane (yellow in figure 4)*

Figure 4 YZ-plane (blue in figure 4)

2 METHODS

2.1 MATERIALS

To implement the segmentation method and to combine and analyse all obtained data, Matlab 2014a and its GUIDE function were used. The method is applied on 20 trans-esophagal echocardiograms (TEEs). All TEEs were obtained on mid esophageal level in one patiënt during a single recording session. During the recordings the thorax was closed. All TEEs were tracked based on Electroctrocardiography (ECG) and contain two cardiac cycles (systole-systole). The data forms a 4-dimensional matrix. The first dimension contains the y-coordinates, the second the x-coordinates and the third the z-coordinates of the field of view. The fourth dimension contains time, forming the separate frames of the TEE recordings.

2.2 MANUAL SEGMENTATION

Figure 3 contains a 3D heart model showing a 2D TEE plane creating a cross section of the mitral valve. The figure demonstrates the orientation of the mitral valve within the heart. The 3D TEE used for this method, consists of a cone-shaped field of view. This field of view contains the left atrium, ventricle and mitral valve. The cone is positioned straight up within the used coordinate system (see figure 4), while the cone is oriented sideways within the heart (see figure 3). The used coordinate system is drawn in both figure 3 and 4.

The mitral annulus is segmented within the xz-plane (yellow) and yz-plane (blue). For each time frame, all slices containing the annulus are evaluated. The attachments of the mitral valve leaflets to the annulus are selected manually. An example of segmentation is given in figure 5 and 6 (white crosses).

2.3 REGISTRATION

To create a dynamic model it is essential that all data (i.e. 3D positions (p)) is comparable. Therefore, registration is needed to place the local TEE coordinate system onto the world coordinate system. Registration consists of three operations, scaling (S), rotation (R) and translation (t):

$$^{W}p = {}^{TEE}R_W\left({}^{TEE}S_W\left({}^{TEE}p - {}^{TEE}t_W\right)\right)$$

First, the scaling is applied. The scaling vector consists of the voxel size and scales the coordinate system to centimetres. The vector is obtained from the DICOM information and is three-dimensional:

$$^{TEE}S_W = \begin{bmatrix} x_{voxel} \\ y_{voxel} \\ z_{voxel} \end{bmatrix}$$

Secondly, a rotation is applied such that the annulus segmented in the first time fragment is oriented horizontally, i.e. placed onto the xy-plane (see figure 7). Hence, this places all segmented annuli of the first timeframe in the same start position and makes the movement comparable. The annuli are placed horizontally by fitting an orthogonal regression using Principal Components Analysis (PCA)[11]. This method uses the segmented coordinates to find a plane for which the sum of squared orthogonal distances is minimized. The fitted plane is showed in figure 7: all green coordinates are located underneath the plane and all red coordinates are above the plane.

PCA uses orthogonal transformation to create principal components from a set of observations. These components are the eigenvectors of the covariance matrix of the data. The components are orthogonal due to the symmetry of this matrix and have a decreasing order: the first component has the largest variance, the last component the smallest variance.

PCA was applied on the segmented annuli. The PCA results in two principal components within the horizontal plane of the annulus. These vector represent the largest and smallest variance in the

segmented coordinates. The cross product of these vectors result in a third vector that is orthogonal to the horizontal plane. The normalised vectors of these three vectors form the rotation matrix of the plane, which

segmented annulus of the first timeframe in the xy-plane.

The found vectors can be oriented into the negative or positive direction. This creates two possibilities rotation matrices. For the
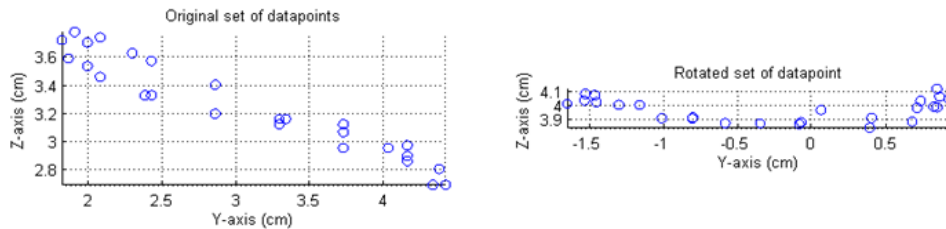

Figure 7 (Left) Original coordinates of segmented annulus, (Right) Rotated coordinates of segmented annulus
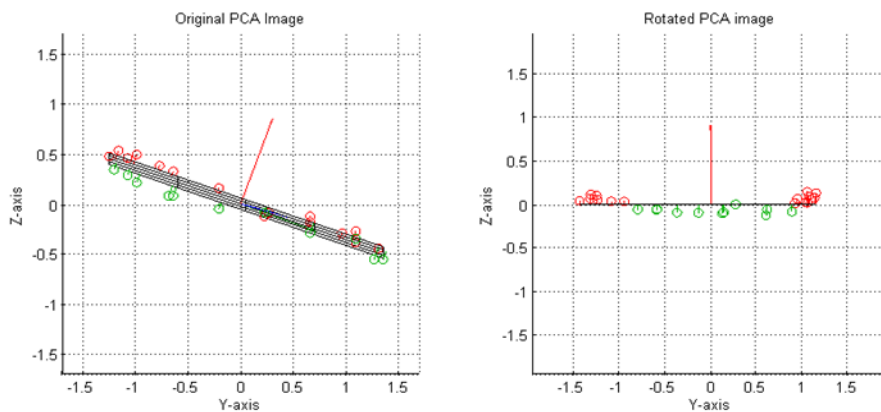

Figure 7 (Left) Plane created by orthogonal regression and rotational vectors fitting the original coordinates of segmented annulus, (Right) Rotated plane and coordinates of the segmented annulus
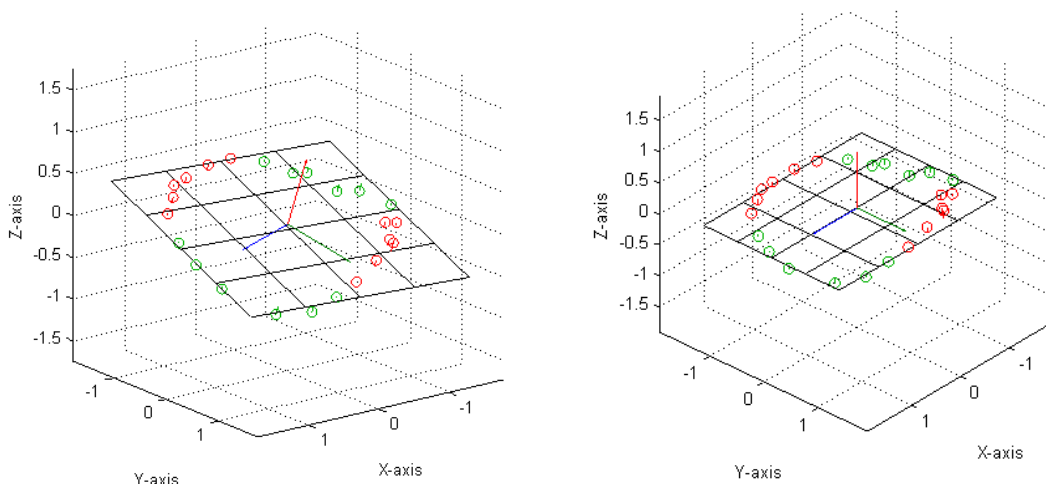

Figure 7 (Left) Original PCA plane showing the long axis and short axis vectors, (Right) Rotated PCA plane showing the short axis vector rotated onto the y-axis and the long axis vector onto the x-axis

is used to rotate all segmented coordinates. This rotation places the

comparison of the data, it is necessary that all coordinates are rotated similarly. Therefore the condition is set that the

5

vectors are only allowed to be orientated into the positive direction. Hereby, the short axis will always be in counter-clockwise position relative to the long axis and the normal vector will point upwards. The rotation matrix forms a 3x3 matrix:

$$^{TEE}\boldsymbol{R}_W = \begin{bmatrix} R_{xx} & R_{xy} & R_{xz} \\ R_{yx} & R_{yy} & R_{yz} \\ R_{zx} & R_{zy} & R_{zz} \end{bmatrix}$$

In this method the translation was not included. This is because the TEEs were recorded in the same patient within one single recording session. It is assumed that the level of the probe in the oesophagus was not changed. This means that the location of the annulus within the coordinate system does not vary between the different recordings.

3 STATISTICAL ANALYSIS AND MODELING

For each timeframe a dataset with coordinates is created forming the segmented annulus. For the analysis, the mean of every segmented annulus is computed (see figure 8). n-recordings and T-timeframes creates a dataset with n x T mean values. For each individual recording (n), the mean of the set of mean values is substracted, creating the zero mean and placing all values around the horizontal axis. This enables comparison of the shape of movement. Finally, for each timeframe (T) the mean and standard deviation for the x-, y- and z-coordinates is computed, creating a mean 3-dimensional movement. These mean values are evaluated with the 'Curve Fitting' function of Matlab.
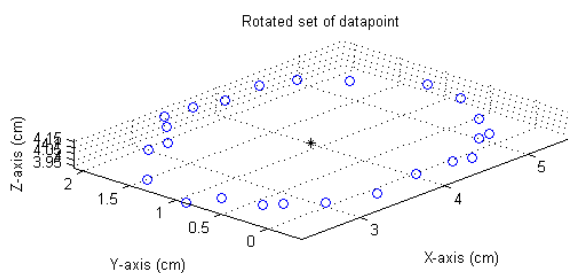

Figure 8 Segmented annulus with plotted mean coordinate

4 RESULTS

Figure 9, 11 and 13 show the movement in the x-, y- and z direction for each segmented annulus. Each color presents a seperate TEE. Time dependancy is eliminated by plotting the displacement over phase. Each phase period of 0 to 360
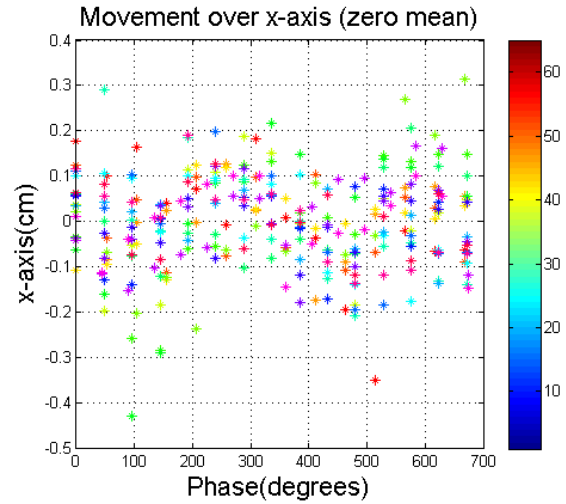

Figure 9 Movement over x for each segmented annulus
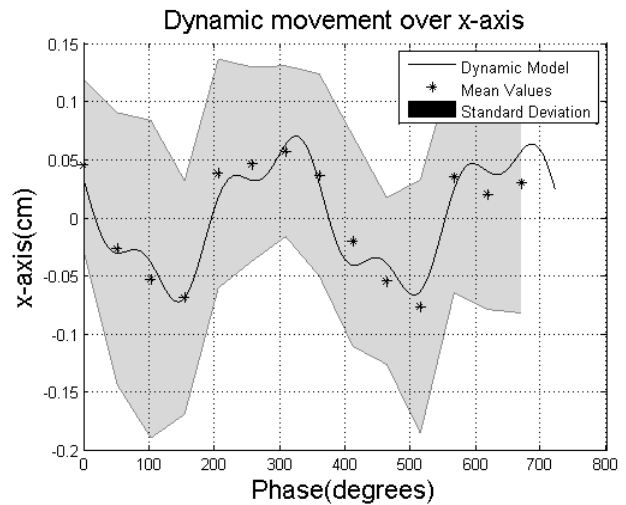
Figure 5 Mean movement over x, including the dynamic model and standard deviation

degrees contains a full cardiac cycle. Figure 10, 12 and 14 show the mean values (μ) of the segmented annuli. Using the curve fitting tool, the most appropriate dynamic models were determined and plotted within the movement plot. Subsequent, the standard deviations (σ) were computed and plotted. The height of the grey area represents $\mu \pm \sigma$.

6

The results for the x- coordinates in figure 11 form a constant broad band with a constant standard deviation represented in figure 12 (0.09-0.14 cm). A pattern could be recognized for which the most appropriate model was plotted in figure 11. This model is a sum of sinusoids with 2 terms and shows a movement range of 0.16 cm in the x-direction. The coefficient of determination (R) of the model is 0.83. Due to the large standard deviation range, the results are expected not to be significant for the creation of a conclusive dynamic model.

The results for the y-coordinates in figure 13 are less consistent than the results for the x- coordinates. The segmented coordinates form broad band at 0 and 700 degrees, yet converge around 400

degrees. This is also represented by the standard deviation in figure 14 (0.07 to 0.22 cm). The standard deviation range is maximal at 0 and 700 degrees and is minimal around 400 degrees. The most appropriate model is plotted in figure 14. This model consists of a sum of sinusoids with 2 terms, showing a movement range of 0.23 cm in y-direction. The model explains 82% of the variance in plotted results. Yet, the results are expected to be not significant enough to create a conclusive dynamic model.

A clear pattern is recognised in the movement over z (see figure 13). The results form a small band and show a sinusoidal signal (see figure 14). The standard deviation forms a small band as well with the range of 0.07 to 0.10 cm. A
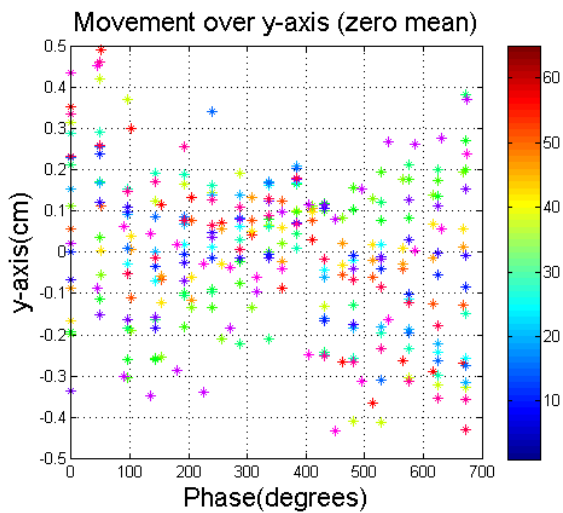

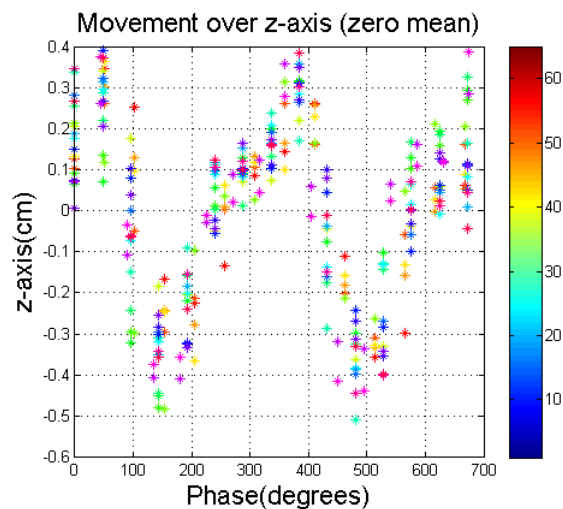Figure 8 Movement over y for each segmented annulus

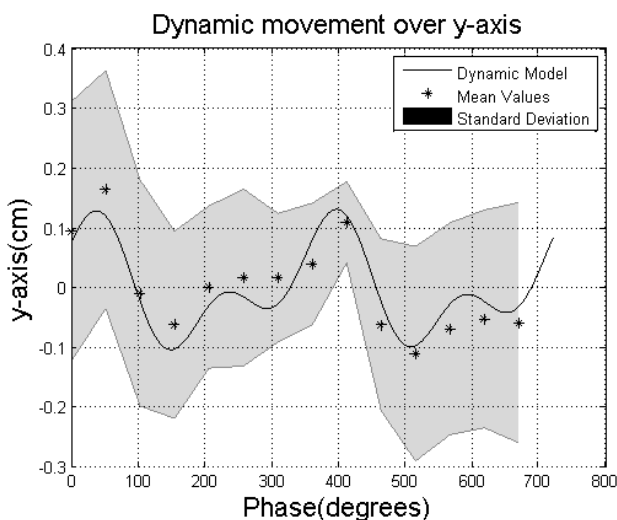Figure 9 Movement over z for each segmented annulus

Figure 7 Mean movement over y, including the dynamic model and standard deviation
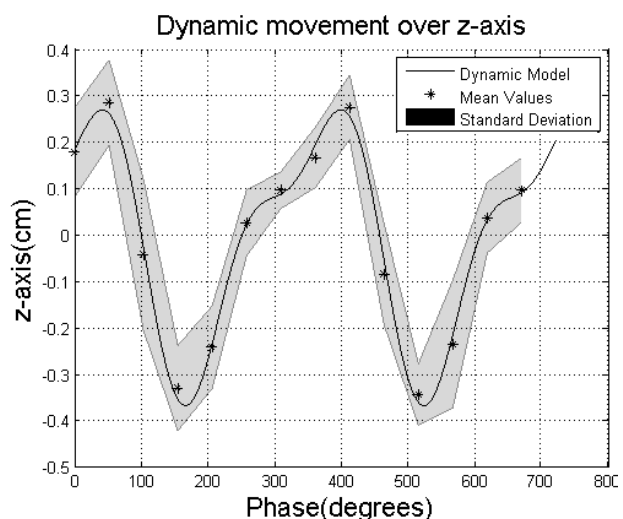

Figure 6 Mean movement over z, including the dynamic model and standard deviation

7

model was established by a Fourier series consisting of 2 terms, defined by:

$$a_0 = -0.01019$$
$$a_1 = 0.267$$
$$b_1 = 0.0171$$
$$a_2 = -0.07464$$
$$b_2 = 0.07621$$
$$\omega = 0.01762$$

$$f(p) = a_0 + a_1 * \cos(p * \omega) + b_1 \\ * \sin(p * \omega) + a_2 \\ * \cos(2 * p * \omega) + b_2 \\ * \sin(2 * p * \omega)$$

With $p = phase$ (degrees)

The coefficient of determination of the model is 1.0 and shows a movement range of 0.64 cm.

The more detailed results are included in the appendices. In figure 16-19 the mean segmented x-, y- and z- coordinates of the individual segmented annuli are shown. Figure 20 shows the total μ and σ for each timeframe.

5 CONCLUSION

Due to large standard deviation ranges in x-direction (0.09-0.14 cm) and y- direction (0.07-0.22 cm) the segmentation data is expected to be insignificant. Hence no conclusive dynamic models were created for the movement in x- and y-direction. The standard deviation in z-direction has the range of 0.07-0.10 cm. The dynamic model for the movement of the annulus in the z-direction forms of a Fourier consisting of 2 terms. The coefficient of deviation of this model is 1.0.

6 DISCUSSION

6.1 TEE

In this research TEEs were used for the manual segmentation of the mitral valve. TEEs are cheap and very useful for the evaluation of the mitral valve[8,12,13]. Also, TEE will be the method of choice for the online tracking during transcatheter surgery of the mitral valve. Therefore, it was preferable to use the TEE for the creation of the dynamic models.

6.2 INCONCLUSIVE RESULTS

Results have shown that the segmentation created inconclusive results for the movement of the annulus in x- and y-direction. Some remarks can be made that might explain why the results were inconclusive.

First, because the heart rests onto the diaphragm, the movement of the annulus is both dependent on the movement of the heart during the heart cycle and the movement created by the diaphragm due to breathing. The movement of the diaphragm is most dominant in x-direction. During the recordings of the 20 TEEs the difference in breathing phase was not taken into account. The location of the mitral valve can differ between the 20 TEEs due to displacement of the diaphragm. This could explain the broad band of data in the x-direction.

Another component leading to the broad banded data could be assigned to the zero-mean method. The data was decreased by its mean value for each TEE. Yet, the computed mean can be inaccurate due to the limited sample frequency. Peak coordinates could be missed when they are reached in between two timeframes. Therefore, the mean will decrease and the signal will be less compensated. This will create differences in the results for the different TEEs.

Adding to this, the variance in data could be attributed to the PCA. The PCA results in two orthogonal principal components within the horizontal plane, for which the first represents the largest variance and the second the smallest variance. Yet, this seems to be a false assumption where the segmented shape of the annulus appears not to be constant and non-ellipsoid. This could be the result of the inaccuracy of the

manual segmentation. When the shape of the annulus is inconsistent the PCA will be inaccurate and the direction of the long and short axis vectors will not be similarly oriented within the different annuli. Also, when the data is circular the PCA will make no distinction between the largest and smallest variance. Therefore, the principal components could switch. The inconsistent shape and the non-ellipsoid aspect of the segmented annuli create differences in the rotation around the z-axis. Hereby, the initial orientation of the annuli within the xy-plane will vary and the x- and y- components of the movement will not fully be separated, which creates variance in data.

In summary, the variance in data could be explained by the movement component due to breathing, the inaccuracy of the mean-zero due to the limited sample frequency and due to the inaccuracy of the PCA. The contribution of the movement due to breathing should be analysed and taken into account. Also, the sample frequency should be increased or an alternative method for the zero-mean should be selected to create comparable data. The restriction of the TEE hardware creates a limited sample frequency, which eliminates the first option at this moment. Finally, the PCA should be improved. This could be established by including a second segmentation, where the user selects the two locations where the mitral leaflets meet within the annulus. The annuli could then be rotated over the z-axis and aligned based on this segmentation.

6.3 NORMALISED TIME

In the results, the displacement is plotted over the phase, where 0 to 360 degrees contains a full heart cycle. The domain 'phase' is preferred over 'time'. During surgery it is possible that the heart rate will vary. It is essential that the dynamic model can be adjusted conform the change in heart rate. This is accomplished by:

$$Time = \frac{phase}{heart\ rate * 360} \quad [s]$$

However, problems could be raised because the heart rate is obtained by sampling, it is not possible to correct for the change in heart rate constantly. When the heart rate changes rapidly, the phase of the model might lag of lead to the actual phase of the motion of the annulus.

6.4 USER INDEPENDENCY

The segmentation method is manual and it is expected that the inter- and intra-independency is high. Figure 5 and 6 show a manual segmentation of the annulus. It is trivial that the location of the actual attachment of the mitral valve is indistinct. For the user it is almost impossible to exactly distinct the attachment and differences between the segmentations will definitely exist. The intra- and inter-user independencies are not evaluated. When the presented method is used to create an actual model, it is recommendable to perform an evaluation on the user independency. The method should be adjusted such that the independency is minimalized.

6.5 ANNULUS DEFORMATIONS

Levack et al. describe that the annulus deforms during the cardiac cycle[9]. This deformation consists of a change in diameter and the annular height. Because the movement is analysed based on the mean coordinates of the segmented annuli, the deformation of the annulus is not taken into account. In future development it is recommendable to include the deformation component in the analysis.

6.6 ROTATION

For each timeframe PCA was applied to compute the rotational matrix for the segmented annulus. This could create information about the rotation of the annulus during the cardiac cycle. However, because the PCA seems not to

be fully accurate this analysis was excluded.

6.7 FUTURE WORK

The final goal is to create a fully automated 3D segmentation method to evaluate and track the movement of the mitral valve. The manual segmentation appears to be inaccurate and is very time consuming[13]. Automated segmentation will provide a method for the offline creation of dynamic models and is essential for the online tracking system. However, three–dimensional automated segmentation of the mitral valve in echocardiographic imaging seems to be challenging[13]. No user-independent segmentation methods for the mitral annulus have been presented yet. Some brief recommendations concerning the development of an automated segmentation method are given below.

The ultrasound images contain noise. To use segmentation techniques such as edge detection or thresholding, it is essential that the speckled noise is reduced[14]. The Gaussian filter seems to be the most appropriate filter for the reduction of noise (see figure 19-20). This filter limits blurring and reduces noise, while preserving the image features.

Even though no full 3D segmentation methods for the mitral annulus have been presented, some potential methods are available. Schneider et al. presented in 2010 a method in which they created a semi-automated 3D segmentation method for the mitral annulus, designed for closed

mitral valves. This method needs a single user-defined point near the centre of the valve. In 2012 Schneider et al. improved this method. They were able to create a method in which the closed state of the annulus could be expected. In other states an optical flow algorithm is used to track the movement of the mitral valve. For this method minimal user-input is needed. Yet, the method should still be improved due to the restricted frame rate that can be used.

Also, active contours forms a potential method for the segmentation of the mitral annulus[15]. This is a group of segmentation methods that uses training phases to create the most optimal segmentation. By creating a database a model for the segmentation could be created, 'teaching' the algorithm to recognise certain structures. These structures could be the fusion of the mitral leaflets with the annulus. However, the use of active contours for the segmentation of the mitral valve has not been evaluated yet. The Lucas-Kanade algorithm forms another potential method for tracking the movement of the mitral annulus. This method uses image alignment to track the movement of specified pixels within different timeframes[16]. It defines that pixels will follow a certain path or track, defined by the optical flow equation. It computes this track for groups of neighbouring pixels. The Lucas-Kanade algorithm is less sensitive to image noise than other segmentation methods, which could be very useful in ultrasound images. It is recommendable to develop and evaluate this method for the tracking of the annulus.
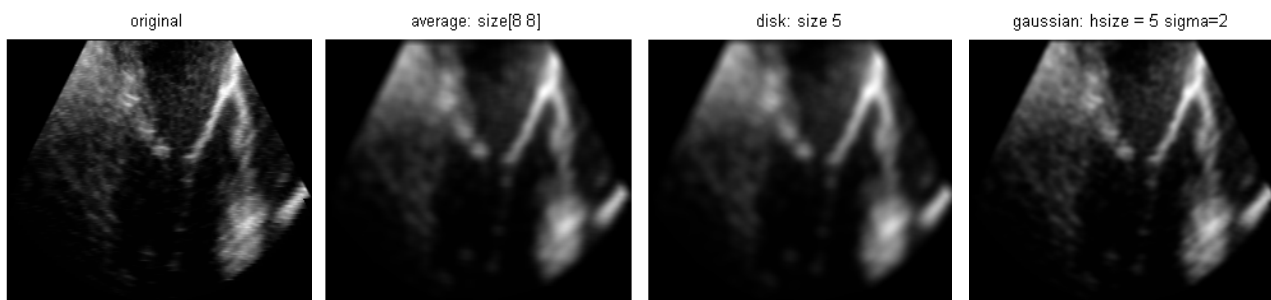

Figure 15 original TEE image (xz-plane)

Figure 15 TEE image filtered by averaging filter

Figure 15 TEE image filtered by a disk convolution

Figure 15 TEE image filtered by a Gaussian filter

REFERENCES

1.   Siregar S, Heer F de, Versteegh RHHGMIM, et al. Trends and outcomes of valve surgery: 16-year results of The Netherslands Cardiac Surgery National Database. *Eur. J. Cardio-Thoracic Surg.* 2014;46(3):386-397. doi:10.1093/ejcts/ezu017.

2.   Cheung A, Webb J, Verheye S, et al. Short-Term Results of Transapical Transcatheter Mitral Valve Implantation for Mitral Regurgitation. *J. Am. Coll. Cardiol.* 2014;64(17):1814-9. doi:10.1016/j.jacc.2014.06.1208.

3.   Anyanwu AC, Adams DH. Transcatheter mitral valve replacement: the next revolution? *J. Am. Coll. Cardiol.* 2014;64(17):1820-4. doi:10.1016/j.jacc.2014.08.024.

4.   Cheung AW, Gurvitch R, Ye J, et al. Transcatheter transapical mitral valve-in-valve implantations for a failed bioprosthesis: A case series. *J. Thorac. Cardiovasc. Surg.* 2011;141(3):711-715. doi:10.1016/j.jtcvs.2010.11.026.

5.   Cheung A, Webb JG, Barbanti M, et al. 5-Year experience with transcatheter transapical mitral valve-in-valve implantation for bioprosthetic valve dysfunction. *J. Am. Coll. Cardiol.* 2013;61(17):1759-1766. doi:10.1016/j.jacc.2013.01.058.

6.   University of Twente. Surgical Robotics Laboratory. 2014. Available at: http://www.surgicalroboticslab.nl/. Accessed September 4, 2012.

7.   Vrooijink GJ, Ellenbroek TTM, Breedveld P, Greandjean JG, Misra S. A preliminary study on using a Robotically-Actuated Delivery Sheath (RADS) for transapical aortic valve implantation. In: *Robotics and Automation (ICRA), 2014 IEEE International Conference on.* Hong Kong: IEEE; 2014:4380-4386. doi:10.1109/ICRA.2014.6907497.

8.   Munin MA, Thierer J, Raggio IM, et al. Three Dimensional Echocardiographic Analysis of Mitral Valve Characteristics Análisis de las características de la válvula mitral en ecocardiograma tridimensional. *Argentine J. Cariol.* 2014;82(4):279-284.

9.   Levack MM, Jassar AS, Shang EK, et al. Three-dimensional echocardiographic analysis of mitral annular dynamics: implication for annuloplasty selection. *Circulation* 2012;126(11 Suppl 1):S183-8. doi:10.1161/CIRCULATIONAHA.111.084483.

10.   Karagiannis SE, Karatasakis GT, Koutsogiannis N, Athanasopoulos GD, Cokkinos D V. Increased distance between mitral valve coaptation point and mitral annular plane: significance and correlations in patients with heart failure. 2003:1174-1178.

11.   Mathworks. Fitting an Othogonal Regression Using Principal Components Analysis. 2014. Available at: http://nl.mathworks.com/help/stats/examples/fitting-an-orthogonal-regression-using-principal-components-analysis.html?refresh=true. Accessed February 19, 2015.

12.   Lang RM, Badano LP, Tsang W, et al. EAE/ASE recommendations for image acquisition and display using three-dimensional echocardiography. *Eur. Heart J. Cardiovasc. Imaging* 2012;13(1):1-46. doi:10.1093/ehjci/jer316.

13.   Schneider RJ, Perrin DP, Vasilyev NV, Marx GR, Nido PJ Del, Howe RD. Mitral Annulus Segmentation From 3D Ultrasound Using Graph Cuts. *IEEE Trans. Med. Imaging* 2010;29(9):1676-1687. doi:10.1109/TMI.2010.2050595.

14.   Lakare S. 3D Segmentation Techniques for Medical Volumes. 2000;65:1-23. doi:10.1.1.200.7315.

15.   Blake A, Isard M. *Active Contours*. 2nd ed. London: Springer; 1998.

16.   Baker S, Matthews I. Lucas-Kanade 20 Years On : A Unifying Framework Part 1 : The Quantity Approximated , the Warp Update Rule , and the Gradient Descent Approximation. *Int. J. Comput. Vis.* 2004;56:221-255. doi:10.1023/B:VISI.0000011205.11775.fd.

17.   Education TGHD of API. Spectal Doppler. :Mitral Valve. Available at: http://pie.med.utoronto.ca/tee/tee_content/TEE_spectral_mitralValve.html. Accessed February 21, 2015.
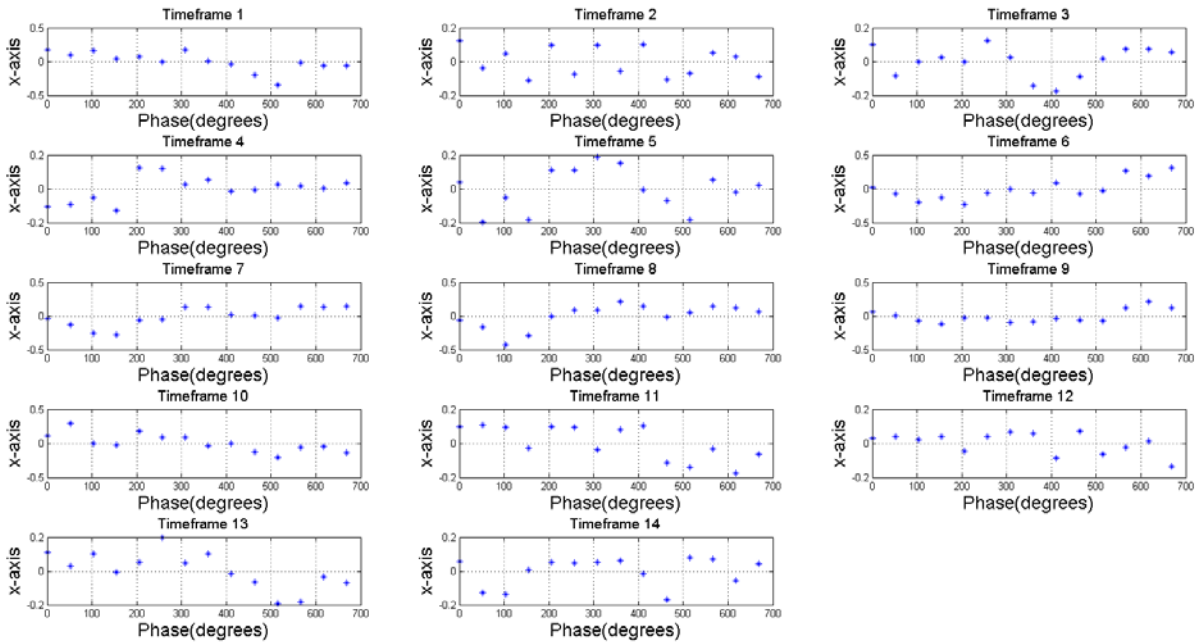
7 APPENDICES

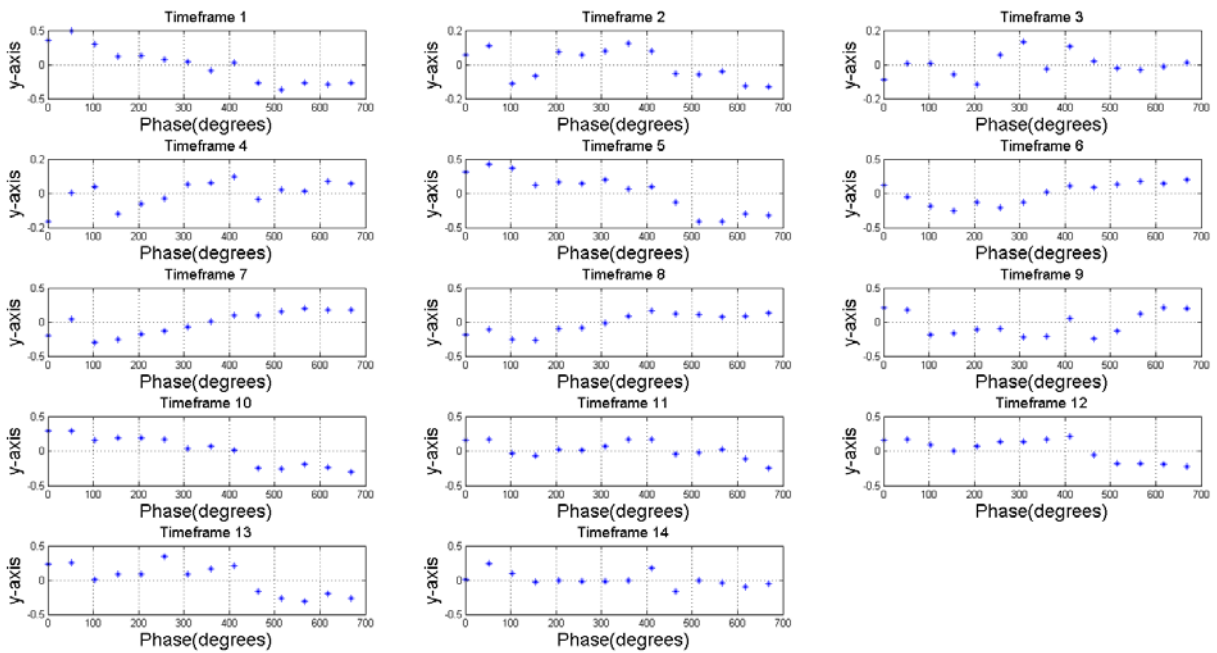*Figure 16 Movement over x for each individual timeframe*

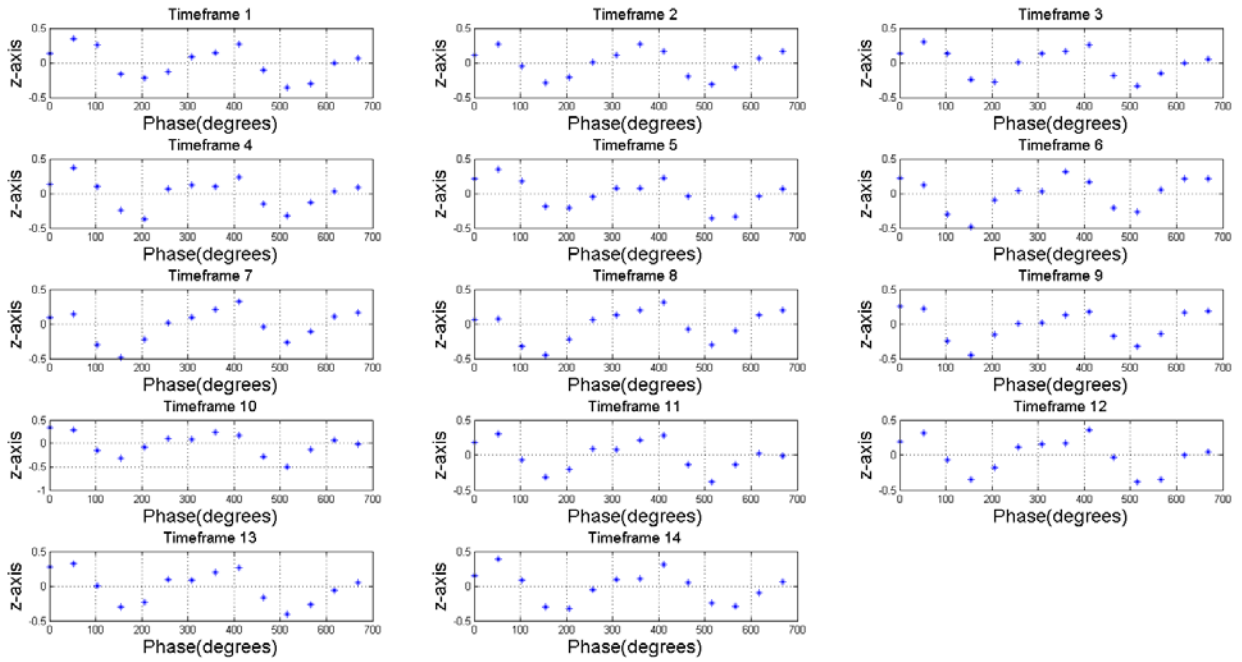*Figure 17Movement over y for each individual timeframe*

Figure 18 Movement over z for each individual timeframe

Timeframe	Mean-X	STD-X	Mean-Y	STD-Y	Mean-Z	STD-Z
1	0	0.073127	0.093502	0.216079	0.176366	0.095949
2	-0.0268	0.116461	0.162976	0.198318	0.283285	0.091474
3	-0.05289	0.135971	-0.00953	0.188205	-0.04319	0.161843
4	-0.06865	0.099897	-0.06224	0.155922	-0.32947	0.091252
5	0.037559	0.097908	0.000629	0.135045	-0.24157	0.088386
6	0.0457	0.083104	0.016487	0.147516	0.025006	0.070652
7	0.0567	0.0731	0.015908	0.107413	0.095476	0.039451
8	0.036347	0.086567	0.03897	0.101384	0.165565	0.06482
9	-0.02045	0.09006	0.108587	0.067606	0.27351	0.068751
10	-0.05445	0.071392	-0.06225	0.143075	-0.08479	0.108403
11	-0.07627	0.10848	-0.11053	0.178689	-0.34321	0.066229
12	0.0346	0.099256	-0.06891	0.176611	-0.23477	0.136947
13	0.019893	0.098685	-0.05244	0.1814	0.036367	0.075906
14	0.029504	0.111399	-0.05884	0.200192	0.09535	0.068955

Figure 19 Mean x-, y-, and z-coordinates with accompanying standard deviation for each time frame